Palaeontology
The Palaeontological Association
www.palass.org

[Palaeontology, Vol. 64, Part 4, 2021, pp. 573–584]

TECHNICAL REPORT

A METHOD FOR MAPPING MORPHOLOGICAL CONVERGENCE ON THREE-DIMENSIONAL DIGITAL MODELS: THE CASE OF THE MAMMALIAN SABRE-TOOTH

by MARINA MELCHIONNA[1], ANTONIO PROFICO[2], SILVIA CASTIGLIONE[1], CARMELA SERIO[3], ALESSANDRO MONDANARO[4], MARIA MODAFFERI[1], DAVIDE TAMAGNINI[5], LUIGI MAIORANO[5], PASQUALE RAIA[1,*], LAWRENCE M. WITMER[6], STEPHEN WROE[7] *and* GABRIELE SANSALONE[7]

[1]Dipartimento di Scienze della Terra, dell'Ambiente e delle Risorse, Università di Napoli Federico II, 80126 Napoli, Italy; pasquale.raia@unina.it
[2]PalaeoHub, Department of Archaeology & Hull York Medical School, University of York, Heslington, UK
[3]Research Centre in Evolutionary Anthropology & Palaeoecology, School of Biological & Environmental Sciences, Liverpool John Moores University, Liverpool, UK
[4]Dipartimento di Scienze della Terra, Università degli studi di Firenze, 50121 Firenze, Italy
[5]Department of Biology & Biotechnologies 'Charles Darwin', University of Rome 'La Sapienza', viale dell'Università 32, 00185 Rome, Italy
[6]Department of Biomedical Science, Heritage College of Osteopathic Medicine, Ohio University, Athens, OH 45701 USA
[7]Function, Evolution & Anatomy Research Lab, Zoology Division, School of Environmental & Rural Science, University of New England, Armidale, NSW 2351 Australia
*Corresponding author

Typescript received 10 August 2020; accepted in revised form 12 March 2021

Abstract: Morphological convergence can be assessed using a variety of statistical methods. None of the methods proposed to date enable the visualization of convergence. All are based on the assumption that the phenotypes either converge, or do not. However, between species, morphologically similar regions of a larger structure may behave differently. Previous approaches do not identify these regions within the larger structures or quantify the degree to which they may contribute to overall convergence. Here, we introduce a new method to chart patterns of convergence on three-dimensional models using the R function *conv.map*. The convergence between pairs of models is mapped onto them to visualize and quantify the morphological convergence. We applied *conv.map* to a well-known case study, the sabre-tooth morphotype, which has evolved independently among distinct mammalian clades from placentals to metatherians. Although previous authors have concluded that sabre-tooths kill using a stabbing 'bite' to the neck, others have presented different interpretations for specific taxa, including the iconic *Smilodon* and *Thylacosmilus*. Our objective was to identify any shared morphological features among the sabre-tooths that may underpin similar killing behaviours. From a sample of 49 placental and metatherian carnivores, we found stronger convergence among sabre-tooths than for any other taxa. The morphological convergence is most apparent in the rostral and posterior parts of the cranium. The extent of this convergence suggests similarity in function among these phylogenetically distant species. In our view, this function is most likely to be the killing of relatively large prey using a stabbing bite.

Key words: morphological convergence, *search.conv*, Felidae, Barbourofelidae, Thylacosmilidae, sabre-tooth carnivore.

CONVERGENCE implies the evolution of functionally analogous body parts shared by distantly related species (Losos 2011; Wake *et al.* 2011) and it remains widely studied and reported in the biological and palaeontological literature. Commonly cited cases include neck elongation in sauropods and giraffes (Sander *et al.* 2010), high-crowned molars in grazing mammals (Janis 2008; Raia *et al.* 2011), the trenchant-heeled condition characterizing the lower molars of hypercarnivorous canids (Van Valkenburgh 2007) and the elongated upper canines (sabres) occurring in a number of carnivorous mammals (Wroe *et al.* 2008). Although an array of different

doi: 10.1111/pala.12542

methods have been proposed to study patterns of convergence (Harmon *et al.* 2005; Stayton 2006; Adams & Collyer 2009; Muschick *et al.* 2012; Ingram & Mahler 2013; Stayton 2015; Castiglione *et al.* 2019) most of these are limited to a simple positive or negative inference. With few exceptions, such as convergence on similar body plans in some fast-swimming marine vertebrates (Lingham-Soliar 2016), studies of morphological convergence have targeted specific body parts (e.g. sabres, long necks, or wings) rather than the larger structures or bodies of which they are part. Excepting a few self-evident cases, currently available methods can determine whether convergence is present, but not identify specific regions within the larger structures and quantify the degree to which they contribute to convergence (McGhee 2011). This may impose limitations when assessing whether convergence is restricted to superficial morphological resemblance, or whether it is a consequence of shared selective pressures (Wainwright 2007; Moen 2019). For instance, by combining finite element analysis and geometric morphometrics to investigate humeral shape in fossorial mammals, Sansalone *et al.* (2020) noted that convergence among digging moles can only be demonstrated when mechanical performance is taken into account with morphology. Almost to the contrary, shared morphologies in sabre-toothed carnivores may obscure a rich functional diversity within the group (Lautenschlager *et al.* 2020). These examples highlight the difference between morphological convergence, which relates to simple phenotypic similarity, and functional convergence, which may take place even without phenotypic resemblance.

We have recently developed a novel and rapid method to address morphological convergence, deployed with the R function *search.conv* (Castiglione *et al.* 2019) embedded in the package RRphylo (Castiglione *et al.* 2018). This approach permits the identification of the pattern between entire clades or across unrelated species sparsely occurring across a phylogeny. The *search.conv* function computes the angle between vectors of principal component (PC) scores retrieved from geometric morphometric (GM) data to assess whether two shapes (vectors of PC scores) are morphologically closer (i.e. have a smaller angle between them) than would be predicted by their phylogenetic distance alone. Since principal component analysis (PCA) ordination of GM data represents both affine and non-affine components of shape variation, identifying the PC axes responsible for the pattern of convergence allows us to chart it on the focal biological shapes, then map and quantify the degree to which individual regions contribute to overall convergence on the structures under study. These concepts are central to the new methodology we present here: *conv.map*.

To illustrate how *conv.map* works, we have applied the method to address a classic example of convergence: the independent evolution of sabre-tooth morphology in mammalian carnivore lineages. All sabre-tooths are defined by the possession of elongated, laterally flattened upper canines (Emerson & Radinsky 1980; Christiansen 2008), which are widely thought to have been applied in the dispatch of relatively large prey (Akersten 1985; McHenry *et al.* 2007).

Variability in skull and postcranial morphology, for example, relative length of the canines and robusticity of the forelimbs, have led researchers to posit differences in killing behaviour between sabre-toothed species (Duckler 1997; Christiansen 2008; Slater & Van Valkenburgh 2008; Christiansen 2011; Figueirido *et al.* 2018). However, most researchers, including those above, have concluded that, notwithstanding these differences, all mammalian sabre-tooths specialized in killing relatively large prey with slashing bites to the neck, as opposed to suffocation through a clamp-and-hold bite that typifies conical toothed cats (Wroe *et al.* 2013; Figueirido *et al.* 2018).

Mechanical modelling has demonstrated that sabre-tooths perform poorly relative to conical toothed predators in lateral shaking of the skull and jaw adductor driven bites, but are better adapted to resist stabbing, dorsoventral 'bites' driven by neck muscles. On the basis of finite element-based studies that have included both conical and sabre-toothed species, a continuum has been proposed wherein sabre-tooths with increasingly longer canines are characterized by an increasing capacity to resist stabbing forces, but a diminishing ability to resist laterally directed forces (McHenry *et al.* 2007; Wroe *et al.* 2013; Figueirido *et al.* 2018). However, some authors have proposed widely disparate killing and feeding behaviours, including killing bites to the belly as opposed to the neck, and diets comprised of internal organs, or blood, as opposed to meat. These suggestions have been proposed for both placental (*Smilodon fatalis*) and metatherian (*Thylacosmilus atrox*) taxa (Merriam & Stock 1932; Akersten 1985; Janis *et al.* 2020). Perhaps the most divergent hypothesis forwarded in recent times suggests that the taxon characterized by the most hypertrophied canines of any sabre-tooth, the metatherian *T. atrox*, was not a predator at all, but a highly specialized scavenger (Janis *et al.* 2020).

If killing and feeding behaviour did differ greatly between sabre-tooth taxa, then we might expect to find that similarities in cranial shape were localized and not shared across the functionally relevant regions of the cranium for all taxa. Our objectives here were therefore to determine how many and to what degree different anatomical regions of the cranium were shared across very distantly related clades, and whether these differences were significant.

To address this question, we applied our methodology to a large sample comprising two placental sabre-tooth families, the single known metatherian sabre-tooth, and a wide range of other carnivorous taxa.

MATERIAL AND METHOD

Data preparation

Thirty-two homologous landmarks were sampled manually on 92 specimens. The landmark configuration defines the shape of the dorsal regions of the cranium, including the maxillary bones and the tooth sockets. We excluded the zygomatic arch from the sampling since in fossil specimens it is rarely preserved. We then placed and slid 1000 bilateral semi-landmarks (500 on each side) automatically using the 'Morpho' R package (Schlager *et al.* 2020). Taxa included a barbourofelid, a dirk-toothed and a scimitar-toothed felid among placentals. We also sampled a range of extant conical toothed cats including *Neofelis* which displays the most morphological features common to extinct sabre-tooths among extant felids (Christiansen 2008). Among metatherians we included the sparassodont *Thylacosmilus atrox*, as well as dasyuromorphians, and the diprotodontian *Thylacoleo carnifex* to provide species phylogenetically close to *Thylacosmilus*. Altogether our data set comprised 49 extant and extinct species (see Melchionna *et al.* 2020, appendix S1 for details).

Taphonomic distortion was present in two fossil specimens (*Barbourofelis fricki*, *Homotherium serum*). We symmetrized these (see Melchionna *et al.* 2020, appendix S1 for details) using the function *retroDeformMesh* (Schlager *et al.* 2018). Procrustes superimposition was applied using generalized Procrustes analysis (GPA), implemented with the *procSym* function of the R package 'Morpho'. GPA rotates, translates and scales landmark configurations to the unit centroid size, that is, the square root of squared differences between landmark coordinates and Centroid coordinates. After GPA, we applied ordination to the aligned coordinates by means of PCA. The resulting PC scores were taken to represent the shape variables.

Searching for convergence

To perform convergence analysis, we implemented the felid tree embedded in the RRphylo package to add the metatherians included in the analysis (see Melchionna *et al.* 2020, appendix S1 for details). We used the tree and shape data to feed the RRphylo package function *search.conv* (Castiglione *et al.* 2019). This function assesses convergence by testing whether phenotypes in distant clades in a phylogenetic tree are more similar to each other than expected from their phylogenetic distance. Phenotypes are represented by vectors of PC scores derived from geometric morphometric data analysis. Since PC axes have a score equal to zero at their intersection, the phenotypic vectors are calculated in relation to the origin of PC axes (the consensus shape in geometric morphometrics) and the angle they form represents a correlation coefficient. The angle actually spans from 0° to 180°. An angle close to 0° means convergence in shapes, whereas angles around 90° means dissimilarity, and angles close to 180° indicate phenotypes evolving in an opposite direction to the consensus. As the function is also able to test for convergence within one state (or more), we applied *search.conv* to the sabre-tooth group to verify the convergence in the skull shape within the category.

Relative warp analysis

The use of *search.conv* enables us to identify species which show convergent phenotypes. For that purpose, using PCA is ideal as it decomposes the variability of the sample into orthogonal axes describing shape variation around the sample mean shape. However, convergence implies large scale, non-affine shape variation which is best inspected by means of PCA of partial warp scores (relative warp analysis, RWA) weighted by a factor $\alpha > 0$ (α spans from $-\infty$ to $+\infty$; at $\alpha = 0$ RWA corresponds to PCA so that the affine and non-affine components of shape variation are not separated, Rohlf 1993; Rohlf & Bookstein 2003). In the case study reported here, we performed RWA using the Morpho function *relWarp* (Schlager *et al.* 2020) setting the α parameter to 1. Then, we extracted the relative warp scores (RW scores) and the relative warps vectors (RWs).

Mapping convergence

We developed the *conv.map* function to visualize the relative intensity of convergence on 3D surfaces. Although we recommend using RWA with α parameter set to 1, we note that RW scores or PC scores could be used. Given two phenotypic vectors ρ_1 and ρ_2 (i.e. vectors of RW scores or PC scores for any two species or group of species found to converge) of length n, the angle α between them is geometrically equivalent to the correlation coefficient between the vectors (Zelditch *et al.* 2012; Castiglione *et al.* 2019). Removing a pair i of corresponding RW scores from both vectors produces the angle α_i between the remaining scores $\rho_{1[-i]}$ and $\rho_{2[-i]}$ of length n−1. If the removed pair of scores is important to phenotypic similarity $\alpha_i < \alpha$, and vice versa. In *conv.map*, pairs of corresponding RW scores are removed one pair at a time, and the angle between the vectors of remaining RWs computed each time. After the entire procedure is accomplished, the resulting angles $\alpha_{[1...n]}$ are collated into a vector, from the largest to the smallest. This vector would be flat if all RWs are equally responsible for the phenotypic distance between the two original shape vectors. However, RWA decomposes shape

variance in orthogonal axes of maximum variation of decreasing importance, so that the vector of ordered $\alpha_{[1...n]}$ typically presents one or two inflection points. The first inflection point sets apart RW axes which contribute the most to the pattern of convergence (so that removing any one of them provides an angle $\alpha_i \ll \alpha$). The second inflection point, if present, identifies the RW axes responsible for the most important shape differences between the two phenotypic vectors. To locate the first inflection point and therefore select the PC axes responsible for convergence, we applied the function *ede* in the R package 'inflection' (Christopoulos 2019). *ede* performs an extreme distance estimator (Christopoulos 2012; Christopoulos 2016) to efficiently locate the inflection points along a curve. By finding the first inflection point the $RW_{conv1,2}$ matrix of $k \times 2$ RW set of scores (one set of k corresponding RW axes for each species) is extracted from the ρ_1 and ρ_2 vectors. This procedure is analogous to the scree plot criterion commonly used for the selection of 'relevant' axes in PCA. It differs from the scree plot in that rather than selecting the PC axes explaining (cumulatively) most of the variance, it selects the $RW_{conv1,2}$ set of scores in ρ_1 and ρ_2 that maximizes their similarity.

To evaluate the statistical significance of the RW axes selection procedure, *conv.map* computes the angle α_{conv} between the two vectors in $RW_{conv1,2}$. Then, 10 000 angles are computed by randomly selecting from ρ_1 and ρ_2 pairs of corresponding RW scores of length k and testing whether α_{conv} is smaller than 5% of the random angles, which is expected to occur if ρ_1 and ρ_2 represent convergent shapes and $RW_{conv1,2}$ effectively represents the subset of RW axes that best account for convergence.

We used $RW_{conv1,2}$ to retrieve a new landmark configuration using the *showPC* function in 'Morpho'. The new configurations (one for each compared group or species) are weighted on the variance responsible for convergence. The function automatically reconstructs a 3D mesh by using the ball-pivoting algorithm (Bernardini *et al.* 1999) as embedded in the *vcgBallPivoting* function in the R package Rvcg (Schlager & Girinon 2017). Starting from the new surfaces, *conv.map* estimates the area differences between corresponding triangles of each 3D mesh and the consensus shape mesh of the original RWA (including all species). If the selected groups (or species) are convergent, they should present the same pattern of variation in the same regions of the 3D surface, as compared to the consensus shape. Convergent areas will therefore show small variation (plotted in colour shades), whereas non convergent regions of the 3D surface will be plotted in white. The same procedure could be generalized to >2 shape vectors at once. In this case, the user has to supplement *conv.map* with a ρ shape vector for each species, and indicate which species were found to converge. Given j species, the function will calculate all the $RW_{conv1..j}$ matrices (one for each pairwise comparison), and selects the RW axes that appear more than once in the $RW_{conv1..j}$ matrices. By default, if $j > 2$ shape vectors are provided, comparisons of convergence mapping are plotted against the consensus shape, alongside pairwise comparisons.

To summarize, the *conv.map* function works as follows:

1. The RW scores responsible for the morphological convergence are selected from ρ_1 and ρ_2 shape vectors.
2. The landmark configurations of the selected species (or means of species groups) are reconstructed using only the RW scores and RWs (the $RW_{conv1,2}$ matrix) responsible for convergence.
3. Triangle meshes of both the landmark configurations referring to ρ_1 and ρ_2; and consensus shape are interpolated using the ball-pivoting algorithm.
4. Each surface referring to ρ_1 and ρ_2 is compared to the consensus shape, and 3D mesh triangles areas differences are computed.
5. The mesh triangle areas referring to $RW_{conv1,2}$ are calculated and plotted on the 3D surfaces.

The function also provides the opportunity to exclude some RW axes from the analysis. That is because, for example, in most cases RW1 mostly captures high-order morphological differences driven by phylogeny and size variation in the sample.

As input data, *conv.map* needs: the data frame with the RW (or PC) scores of each group or species to be compared (ρ_1 and ρ_2 *dataset*); the matrix of RW (or PC) vectors; the consensus configuration (*mshape*); the number of the RW (or PC) that will be excluded from the comparison, if needed (*exclude* = NULL as default setting) (Table 1).

The function returns the index of the RW axes selected in $RW_{conv1,2,}$ the angle α between ρ_1 and ρ_2, the angle α_{conv} between the two vectors in $RW_{conv1,2,}$ the angle difference $\alpha - \alpha_{conv}$, the p value for $\alpha_{conv;}$ and plots the 3D surfaces coloured according to the convergence pattern represented by $RW_{conv1,2}$ (Table 2).

Applications of conv.map *to sabre-tooths*

To chart convergence on sabre-tooth mammals, we first computed mean RW scores for all species in the tree. We treated *Barbourofelis*, *Homotherium*, *Smilodon* and *Thylacosmilus* as sabre-tooths and ran *search.conv* using all PCs as the multivariate dataset representing shape. Alternative classifications of sabre-tooths failed to find convergence for *Neofelis* and *Yoshi*, despite the fact that they are frequently cited as either showing traits shared with sabre-tooths (the former) or belong to the machairodontinae family (the latter). Then, we used *conv.map* starting from a RWA with $\alpha = 1$ to perform a pairwise comparison between sabre-tooths and the consensus shape. We further compared *Barbourofelis fricki* against machairodont

TABLE 1. Explanation of *conv.map* arguments.

Argument name	Explanation
dataset	Data frame (or matrix) with the RW (or PC) scores of the group or species to be compared
pcs	RW (or PC) vectors of all the samples
mshape	The consensus configuration
conv	A named character vector indicating convergent species as ('conv' in 'dataset') and not convergent species ('noconv')
exclude	Integer: the index number of the RW (or PC) to be excluded from the comparison
out.rem	Logical: if TRUE triangles with outlying area difference are removed
show.consensus	Logical: if TRUE, the consensus configuration is included in the comparison
plot	Logical: if TRUE, the pairwise comparisons are plotted; for more than 5 pairwise comparisons, the plot is not shown
col	Character: the colour for the plot
names	Logical: if TRUE, the names of the groups or species are displayed in the 3D plot

TABLE 2. Explanation of *conv.map* returned values.

Value	Explanation
angle.compare	Data frame including the real angles α between the given shape vectors, the angles α_{conv} computed between vectors of the selected RWs (or PCs), the angles between vectors of the non-selected RWs (or PCs), the difference $\alpha - \alpha_{conv}$, and its *p*-values
selected.pcs	RWs (or PCs) axes selected for convergence
average.dist	Symmetrical matrix of pairwise distances between 3D surfaces
surfaces1	List of coloured surfaces; if two meshes are given, it represents convergence between mesh A and B charted on mesh A
surfaces2	List of coloured surfaces; if two meshes are given, it represents convergence between mesh A and B charted on mesh B
scale	The value used to set the colour gradient, computed as the maximum of all differences between each surface and the mean shape

cats (averaging the shapes of *Smilodon* and *Homotherium*) and against *Thylacosmilus atrox*.

RESULTS

The *search.conv* analysis revealed that among carnivores, only species within the sabre-tooth category displayed significant convergence (mean angle = 43.88°; $p = 0.017$). The pairwise angle comparison between *Barbourofelis*, *Homotherium*, *Smilodon* and *Thylacosmilus* is reported in Table 3A. The angle differences (angles computed between scores vectors of the selected RWs against angles between vectors of the non-selected RWs) of all the convergent groups comparisons are significant, while the comparison with the consensus shape is marginally or not significant for each of the sabre-tooths (Table 3A). *Barbourofelis fricki* and *Homotherium serum* have the lowest distances among all pairwise comparisons, which is also evident in the convergence plots (Fig. 1). All sabre-toothed carnivores are equally distant from the consensus shape (Table 3B). The 3D surfaces comparison reveals a marked similarity in the premaxillary and carnassial areas, and in the occipital region on and around the nuchal crest. The difference pattern against the consensus is similar for all sabre-tooth taxa (Fig. 1).

When *Barbourofelis*, the average machairodont cat skull, *Thylacosmilus*, and the consensus shapes are compared to each other, the angle differences for the convergent species are the only statistically significant (or marginally significant) example detected (Table 4A). The average area difference between *Barbourofelis fricki* and the machairodont cats is the smallest, with surfaces showing great affinity in overall shape. *Thylacosmilus atrox* is closer to *Barbourofelis fricki* than to the machairodonts, with a marked similarity in the muzzle area. All groups are distant from the consensus shape (Table 4B, Fig. 2).

DISCUSSION

Convergence is an evolutionary pattern whereby species belonging to distant lineages develop similar structures to perform the same function (Wainwright 2007; Wroe & Milne 2007; Losos 2011; McGhee 2011). Although a variety of methods have been proposed to test for this pattern (Stayton 2006; Arbuckle *et al.* 2014; Speed & Arbuckle 2016; Castiglione *et al.* 2019), they have invariably focused on the recognition of its statistical significance, making the assumption that the shapes under scrutiny contribute isotropically as a whole. However, the evolution of convergent functions may trace to different morphological trajectories (i.e. one to many mapping, Alfaro *et al.* 2005; Serb *et al.* 2017; Renaud *et al.* 2018) and convergence may fail to apply when the objects' functional performance is ignored (Sansalone *et al.* 2020) meaning that the structural properties of the study objects must be acknowledged (Janis *et al.* 2020). Revealing such particularities is possible by inspecting how different areas of the study objects contribute to the pattern of convergence. This is the aim of the current study. By rendering a visual representation of the relative contribution to

TABLE 3. Pairwise comparisons between *Barbourofelis*, *Homotherium*, *Smilodon*, *Thylacosmilus* and the consensus shape: A, pairwise angle comparison; B, pairwise average area differences, rescaled from 0 to 1.

A	Real angle	Selected	Others	Angle difference	*p*-value
Smilodon–Thylacosmilus	53.351	14.929	143.828	−128.899	<0.001
Barbourofelis–Homotherium	28.620	15.326	64.012	−48.686	<0.001
Homotherium–Smilodon	23.460	20.467	33.301	−12.834	0.061
Barbourofelis–Thylacosmilus	48.382	24.667	117.860	−93.192	<0.001
Barbourofelis–Smilodon	36.887	26.532	76.896	−50.364	0.010
Homotherium–Thylacosmilus	59.022	27.838	138.987	−111.149	<0.001
Barbourofelis–consensus	81.170	45.770	84.033	−38.263	0.067
Thylacosmilus–consensus	87.711	54.637	95.968	−41.331	0.090
Homotherium–consensus	83.943	61.016	86.508	−25.492	0.354
Smilodon–consensus	85.859	66.651	89.063	−22.412	0.366

B	*Barbourofelis*	*Homotherium*	*Smilodon*	*Thylacosmilus*	Consensus
Barbourofelis	–	0.053	0.069	0.080	0.213
Homotherium	0.053	–	0.066	0.112	0.172
Smilodon	0.069	0.066	–	0.075	0.205
Thylacosmilus	0.080	0.112	0.075	–	0.248
consensus	0.213	0.172	0.205	0.248	–

Real angle, the real angle between the given score vectors; Selected, the angles computed between scores vectors of the selected relative warp vectors (RWs); Others, the angles computed between scores vectors of the non-selected RWs; Angle difference, the difference between Selected and Other angle values; *p*-value, the statistical significance of the difference in angle between the selected and non-selected RWs.

convergence of different areas of the biological objects under consideration, *conv.map* helps to identify the morphological regions which may have important implications for functional convergence.

Because of its complexity and multipurpose functioning, the vertebrate skull represents an ideal study object to identify and quantify convergence. In the present study the only example of significant morphological convergence we detected within our sample was the sabre-tooth ecomorph. These four taxa share more anatomical features than any of other carnivore groups, suggesting that the influence of a strong selective pressure drove the iterated evolution of shared morphological features. The *conv.map* method revealed a range of shared anatomical features of particular importance. These were in the premaxillary area, the carnassial region, and in the occipital region around the nuchal crest, which were common to all sabre-tooth carnivores despite considerable phylogenetic distances, particularly with respect to *Thylacosmilus*. These areas are likely to enable the peculiar sabre-tooth killing behaviour, requiring masticatory muscle reorientation, strong neck musculature, low condyles and large gape to effectively use the infamous sabres. In our view this strongly supports the consensus view that despite some anatomical differences and possible functional diversification within sabre-tooths (Lautenschlager *et al.* 2020), the sabre-tooth morphotype universally confers a broadly comparable capacity to hunt and rapidly kill relatively large prey by applying a stabbing bite to the throat assisted by powerful neck muscles (Emerson & Radinsky 1980; Wroe *et al.* 2013), although this specialization may have led to their extinction at different times and locations when large prey became less abundant (Piras *et al.* 2018). Similarities in the rostral and dental areas are likely to represent functional adaptation related to relatively high loadings to which the muzzle was exposed when delivering these stabbing bites. In keeping with this, we found that convergence in sabre-tooths involves the facial region of the skull (particularly in the premaxillary and carnassial area). We also found close similarities in the morphology of occipital area, which was involved in extensive neck muscle depression of the cranium and pull in all sabre-tooths relative to other morphotypes (Duckler 1997; Christiansen 2008). The neurocranium, nasals, and maxillary regions show no bearing on convergence among sabre-tooths and set *Thylacosmilus* apart (Table 4, Fig. 2). Intriguingly, the barbourofelid *Barbourofelis* sits closer to the felid *Homotherium* than it does to *Smilodon*, probably because of similarity in their incisor arcades (Biknevicius *et al.* 1996). We detected greater similarity between *Thylacosmilus* and *Barbourofelis*, suggesting that the metatherian sabre-tooth converged more completely on the highly specialized barbourofelid. Previous work has suggested that these taxa converge on the presence of very long canines, a postorbital bar, mandibular flanges and a number of postcranial characters (Prevosti *et al.* 2012).

FIG. 1. Visualization of the pairwise comparisons of *Barbourofelis*, *Homotherium*, *Smilodon*, *Thylacosmilus*, and the consensus configuration. The colour gradient indicates area differences between the two surfaces. Blue indicates no difference (scale bar rescaled into the range 0–1). In each case, differences between the two taxa are displayed on a reconstruction of the taxon named on the left.

Our findings support the hypothesis that the patterns of convergence on the sabre-tooth cranium provided by the *conv.map* method indicate first-order functional significance, although secondary functional diversity may take place among sabre-tooths (Lautenschlager *et al.* 2020). The absence of convergence in the neurocranium and nasal area is consistent with previously identified features that are not indicative of prey choice or killing method (e.g. the smaller brain of the metatherian *Thylacosmilus*).

The most obvious example here is that the most phylogenetically distant of sabre-tooth taxa, *Thylacosmilus*, is strongly convergent on placental sabre-tooths across regions of the cranium widely considered to be functionally significant. However, a recent study addressing the mechanical performance of *Thylacosmilus* (Janis *et al.* 2020) proposes a very different ecology. Their FEA-based analysis suggested a greater capacity to exert pulling forces in *Thylacosmilus* than in *Smilodon*. It was inferred

TABLE 4. Pairwise comparisons between *Barbourofelis*, machairodont cats (average of *Homotherium* plus *Smilodon*), *Thylacosmilus* and the consensus shape: A, pairwise angle comparison; B, pairwise average area differences, rescaled from 0 to 1.

A	Real angle	Selected	Others	Angle difference	*p*-value
Barbourofelis–*Thylacosmilus*	48.382	3.941	93.912	−89.971	0.009
Barbourofelis – Machairodont cats	12.455	7.300	18.475	−11.175	0.073
Machairodont cats – *Thylacosmilus*	51.846	11.241	103.093	−91.852	0.012
Thylacosmilus–consensus	87.711	51.603	94.427	−42.824	0.285
Barbourofelis–consensus	81.170	55.544	81.629	−26.085	0.413
Machairodont cats – consensus	82.141	62.844	81.833	−18.989	0.474

B	*Barbourofelis*	Machairodont cats	*Thylacosmilus*	Consensus
Barbourofelis	–	0.039	0.054	0.347
Machairodont cats	0.039	–	0.085	0.308
Thylacosmilus	0.054	0.085	–	0.371
Consensus	0.347	0.308	0.371	–

Real angle, the real angle between the given score vectors; Selected, the angles computed between scores vectors of the selected relative warp vectors (RWs); Others, the angles computed between scores vectors of the non-selected RWs; Angle difference, the difference between Selected and Other angle values; *p*-value, the statistical significance of the difference among the angles between the selected and non-selected RWs.

on this basis that *Thylacosmilus* did not deploy killing behaviour common to other sabre-tooths that distinguished them from conical-toothed predators and that it may have been a scavenger. We do not contest the possibility that *Thylacosmilus* was better adapted to exert pulling behaviour, because the only other FEA-based study to include these two taxa did not apply a neck-pulling load case (Wroe *et al.* 2013). On the other hand, we do note that the study of Janis *et al.* (2020) did not include any conical-toothed taxa by way of comparison, whereas the earlier study (Wroe *et al.* 2013) included the conical-toothed *Panthera pardus*. Wroe *et al.* (2013) found that *Thylacosmilus* was better adapted to deliver a stabbing bite that was reliant on head depressing neck musculature than was *Smilodon*, but that both were superior in this respect to *Panthera pardus*. We suggest that *Thylacosmilus* was better adapted to deliver both neck-driven head pulling and depressing functions, but without applying a head-pull load case to a conical-toothed cat as well as to other sabre-tooths there is no mechanics-based evidence to indicate whether a capacity to deliver a head pull is a further defining feature of sabre-tooths or not. As well as FEA-based analysis, an intriguing feature of *Thylacosmilus* identified by Janis *et al.* (2020), determined on the basis of dental microwear patterns, was that *Thylacosmilus* did not habitually consume meat or bone. This raises the possibility that the metatherian sabre-tooth's diet was largely restricted to soft internal organs such as the heart, lungs and liver. These characteristics would make *Thylacosmilus* truly unique among mammalian scavengers, which typically do consume both bone and meat, as well as internal organs. However, large extant mammalian predators commonly consume these internal organs preferentially over meat and bone (Schaller 1972). We consider it more likely that *Thylacosmilus* may have concentrated on the internal organs of prey it had killed, rather than the carcasses of animals killed by other large South American carnivores (e.g. phorusrhacid birds), which were unlikely to have eaten only meat and/or bone and left the internal organs untouched. Sabre-tooths are characterized by relatively weak jaw closing muscles but large head depressors (Wroe *et al.* 2005; Christiansen 2011). *Thylacosmilus* is extreme with regard to both features (Wroe *et al.* 2013), and we contend that together with the evidence for a diet comprised largely of soft internal organs, these characteristics point to an even more extreme example of sabre-tooth killing and feeding behaviour, as opposed to an entirely divergent ecomorph and diet.

CONCLUSION

The use of three-dimensional models has revolutionized the study of fossils in both palaeontology and palaeoanthropology (Cunningham *et al.* 2014). In morphometric analyses, the implementation of geometric morphometric techniques based on 3D configurations has driven the development of new protocols and software suitable for 3D surfaces. These new technologies allow researchers to virtually restore and realign disarticulated elements (Gunz

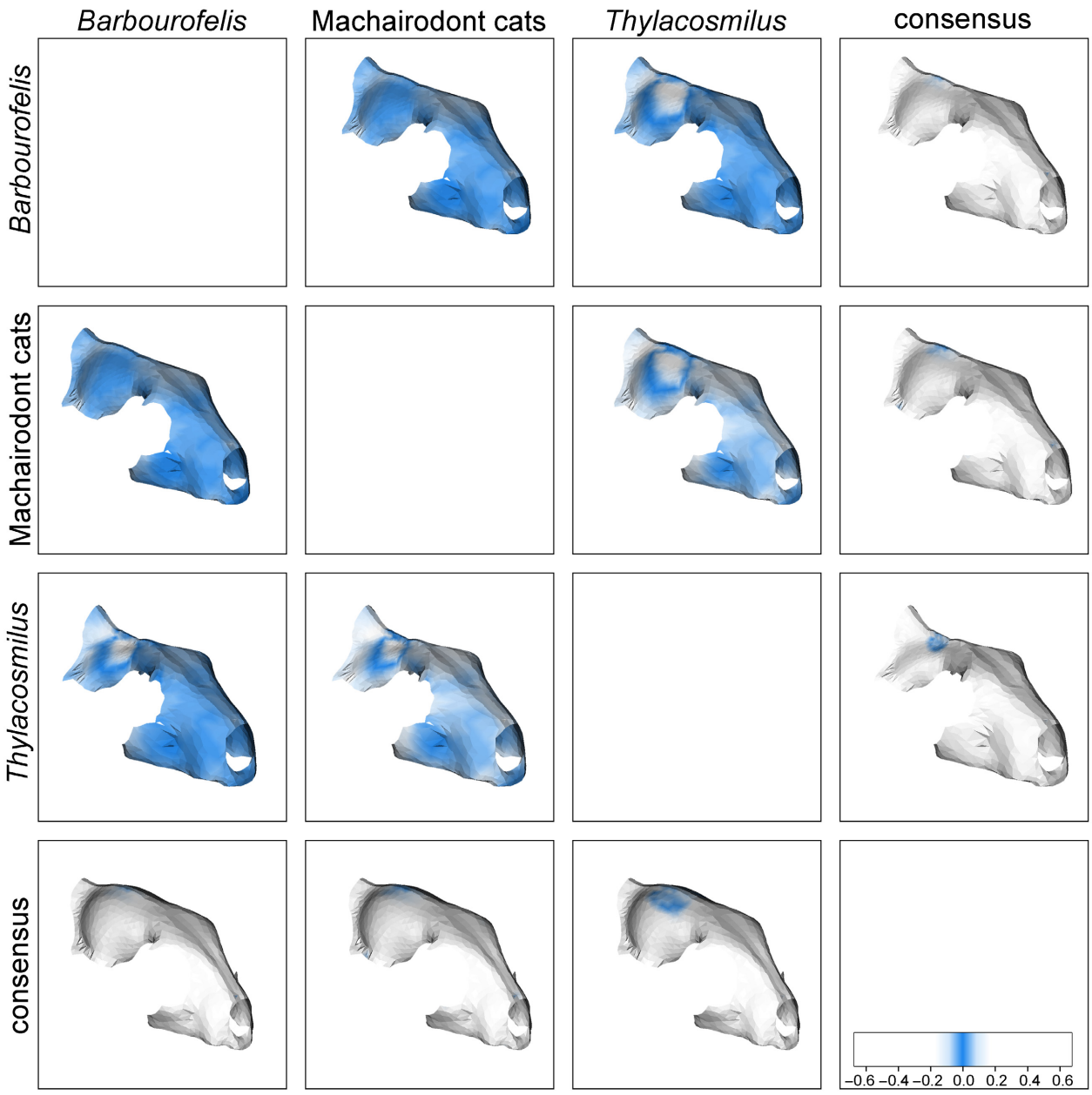

FIG. 2. Visualization of the pairwise comparison between *Barbourofelis*, machairodont cats (*Homotherium* plus *Smilodon*), *Thylacosmilus* and the consensus configuration. The colour gradient indicates area differences between the two surfaces. Blue indicates no difference (scale bar rescaled into the range 0–1). In each case, differences between the two taxa are displayed on a reconstruction of the taxon named on the left.

et al. 2009; Profico *et al.* 2019), and perform the retrodeformation of fossils (i.e. the process of removing distortions in fossils caused by taphonomic forces; Schlager *et al.* 2018) which now permit studying the functional and evolutionary aspects of 3D shape evolution with increased sampling and precision. Here we present a new implementation, named *conv.map*, which allows us to study how patterns of convergence unfold across 3D surfaces. By mapping the regions responsible for the pattern, *conv.map* allows us to visualize and ascertain the functional significance of convergence of the biological structures under scrutiny.

Acknowledgements. We are grateful to Stephan Lautenschlager and an anonymous reviewer for providing important advice. 79 specimens included in the present study are from the PhD database of DT, whose PhD project received support from the 'Avvio alla Ricerca 2019' funding which is financed by the University of

Rome 'La Sapienza'. DT also received support from the SYNTHESYS Access programme that is financed by the European Community Research Infrastructure Action under the FP7 (ES-TAF-2750 awarded to DT). LMW acknowledges support from the United States National Science Foundation (IOB-0517257, IOS-1050154, IOS-1456503). We owe a huge debt of thanks to all curators, collection managers and staff, whose help and support was fundamental for the sampling operations. In particular, with anticipated apologies for certainly forgetting to explicitly mention several of the many people to whom thanks are owed, we want to thank: Susana Fraile, Jorge Morales, Géraldine Veron, Aurélie Verguin, Riccardo Castiglia, Cristiano Dal Sasso, Pierfilippo Cerretti, Adriano De Faveri, Saverio Bartolini Lucenti, Paolo Agnelli, Tony Parker, Itatí Olivares, Agustín Ruella and Eulàlia Garcia Franquesa. We also want to thank Denis Geraads and Nikolai Spassov for providing DT with a copy of their 3D model of *Y. garevskii*.

Author contributions. MM and DT contributed equally. MM, AP, and PR conceived the study. MM, AP, PR, and SC prepared the code. MM, GS, DT, LW, AM and MMod contributed to collection and preparation of the study sample. MM, SW and PR lead the writing. All the authors contributed to the preparation of the manuscript.

DATA ARCHIVING STATEMENT

Data for this study are available in the Dryad Digital Repository: https://doi.org/10.5061/dryad.9kd51c5g6

Editor. Laura Porro

REFERENCES

ADAMS, D. C. and COLLYER, M. L. 2009. A general framework for the analysis of phenotypic trajectories in evolutionary studies. *Evolution*, **63**, 1143–1154.

AKERSTEN, W. A. 1985. Canine function in *Smilodon* (Mammalia; Felidae; Machairodontinae). *Natural History Museum of Los Angeles County*, Contributions in Science, **356**, 1–22.

ALFARO, M. E., BOLNICK, D. I. and WAINWRIGHT, P. C. 2005. Evolutionary consequences of many-to-one mapping of jaw morphology to mechanics in labrid fishes. *The American Naturalist*, **165**, E140–E154.

ARBUCKLE, K., BENNETT, C. M. and SPEED, M. P. 2014. A simple measure of the strength of convergent evolution. *Methods in Ecology & Evolution*, **5**, 685–693.

BERNARDINI, F., MITTLEMAN, J., RUSHMEIER, H., SILVA, C. and TAUBIN, G. 1999. The ball-pivoting algorithm for surface reconstruction. *IEEE Transactions on Visualization & Computer Graphics*, **5** (4), 349–359.

BIKNEVICIUS, A. R., VAN VALKENBURGH, B. and WALKER, J. 1996. Incisor size and shape: implications for feeding behaviors in saber-toothed "cats". *Journal of Vertebrate Paleontology*, **16** (3), 510–521.

CASTIGLIONE, S., TESONE, G., PICCOLO, M., MELCHIONNA, M., MONDANARO, A., SERIO, C., DI FEBBRARO, M. and RAIA, P. 2018. A new method for testing evolutionary rate variation and shifts in phenotypic evolution. *Methods in Ecology & Evolution*, **9**, 974–983.

—— SERIO, C., TAMAGNINI, D., MELCHIONNA, M., MONDANARO, A., DI FEBBRARO, M., PROFICO, A., PIRAS, P., BARATTOLO, F. and RAIA, P. 2019. A new, fast method to search for morphological convergence with shape data. *PLoS One*, **14** (12), e0226949.

CHRISTIANSEN, P. 2008. Evolutionary convergence of primitive sabertooth craniomandibular morphology: the clouded leopard (*Neofelis nebulosa*) and *Paramachairodus ogygia* compared. *Journal of Mammalian Evolution*, **15**, 155–179.

—— 2011. A dynamic model for the evolution of sabrecat predatory bite mechanics. *Zoological Journal of the Linnean Society*, **162**, 220–242.

CHRISTOPOULOS, D. T. 2012. Developing methods for identifying the inflection point of a convex/concave curve. *arXiv*, 1206.5478.

—— 2016. On the efficient identification of an inflection point. *International Journal of Mathematics & Scientific Computing*, **6** (1), 2231–5330.

—— 2019. inflection: Finds the inflection point of a curve. R package v.1.3.5. https://cran.r-project.org/package=inflection

CUNNINGHAM, J. A., RAHMAN, I. A., LAUTENSCHLAGER, S., RAYFIELD, E. J. and DONOGHUE, P. C. J. 2014. A virtual world of paleontology. *Trends in Ecology & Evolution*, **29**, 347–357.

DUCKLER, G. L. 1997. Parietal depressions in skulls of the extinct saber-toothed felid *Smilodon fatalis*: evidence of mechanical strain. *Journal of Vertebrate Paleontology*, **17**, 600–609.

EMERSON, S. B. and RADINSKY, L. 1980. Functional analysis of sabertooth cranial morphology. *Paleobiology*, **6**, 295–312.

FIGUEIRIDO, B., LAUTENSCHLAGER, S., PÉREZ-RAMOS, A. and VAN VALKENBURGH, B. 2018. Distinct predatory behaviors in scimitar- and dirk- toothed sabertooth cats. *Current Biology*, **28**, 3260–3266.

GUNZ, P., MITTEROECKER, P., NEUBAUER, S., WEBER, G. W. and BOOKSTEIN, F. L. 2009. Principles for the virtual reconstruction of hominin crania. *Journal of Human Evolution*, **57**, 48–62.

HARMON, L. J., KOLBE, J. J., CHEVERUD, J. M. and LOSOS, J. B. 2005. Convergence and the multidimensional niche. *Evolution*, **59**, 409–421.

INGRAM, T. and MAHLER, D. L. 2013. SURFACE: detecting convergent evolution from comparative data by fitting Ornstein-Uhlenbeck models with stepwise Akaike information criterion. *Methods in Ecology & Evolution*, **4**, 416–425.

JANIS, C. 2008. An evolutionary history of browsing and grazing ungulates. 21–45. *In* GORDON, I. J. and PRINS, H. H. T. (eds). *The ecology of browsing and grazing*. Springer.

—— FIGUEIRIDO, B., DESANTIS, L. and LAUTENSCHLAGER, S. 2020. An eye for a tooth: *Thylacosmilus* was not a marsupial "saber-tooth predator". *PeerJ*, **8**, e9346-36.

LAUTENSCHLAGER, S., FIGUEIRIDO, B., CASHMORE, D. D., BENDEL, E. M. and STUBBS, T. L. 2020. Morphological convergence obscures functional diversity in

sabre-toothed carnivores. *Proceedings of the Royal Society B*, **287**, 20201818.

LINGHAM-SOLIAR, T. 2016. Convergence in thunniform anatomy in lamnid sharks and Jurassic ichthyosaurs. *Integrative & Comparative Biology*, **56**, 1323–1336.

LOSOS, J. B. 2011. Convergence, adaptation, and constraint. *Evolution*, **65**, 1827–1840.

McGHEE, G. R. 2011. *Convergent evolution: Limited forms most beautiful*. MIT Press.

McHENRY, C. R., WROE, S., CLAUSEN, P. D., MORENO, K. and CUNNINGHAM, E. 2007. Supermodeled sabercat, predatory behavior in *Smilodon fatalis* revealed by high-resolution 3D computer simulation. *Proceedings of the National Academy of Sciences*, **104**, 16010–16015.

MELCHIONNA, M., PROFICO, A., CASTIGLIONE, S., SERIO, C., MONDANARO, A., MODAFFERI, M., TAMAGNINI, D., MAIORANO, L., RAIA, P., WITMER, L. M., WROE, S. and SANSALONE, G. 2020. Data from: A method for mapping morphological convergence on three-dimensional digital models: the case of the mammalian saber-tooth. *Dryad Digital Repository*. https://doi.org/10.5061/dryad.9kd51c5g6

MERRIAM, J. C. and STOCK, C. 1932. The Felidae of Rancho La Brea. Carnegie Institution of Washington Publication, Publication **422**.

MOEN, D. S. 2019. What determines the distinct morphology of species with a particular ecology? The roles of many-to-one mapping and trade-offs in the evolution of frog ecomorphology and performance. *The American Naturalist*, **194**, E81–E95.

MUSCHICK, M., INDERMAUR, A. and SALZBURGER, W. 2012. Convergent evolution within an adaptive radiation of cichlid fishes. *Current Biology*, **22**, 2362–2368.

PIRAS, P., SILVESTRO, D., CAROTENUTO, F., CASTIGLIONE, S., KOTSAKIS, A., MAIORINO, L., MELCHIONNA, M., MONDANARO, A., SANSALONE, G., SERIO, C., VERO, V. A. and RAIA, P. 2018. Evolution of the sabertooth mandible: a deadly ecomorphological specialization. *Palaeogeography, Palaeoclimatology, Palaeoecology*, **496**, 166–174.

PREVOSTI, F. J., TURAZZINI, G. F., ERCOLI, M. D. and HINGST-ZAHER, E. 2021. Mandible shape in marsupial and placental carnivorous mammals: a morphological comparative study using geometric morphometrics. *Zoological Journal of the Linnean Society*, **164**, 836–855.

PROFICO, A., BUZI, C., DAVIS, C., MELCHIONNA, M., VENEZIANO, A., RAIA, P. and MANZI, G. 2019. A new tool for digital alignment in virtual anthropology. *The Anatomical Record*, **302**, 1104–1115.

RAIA, P., CAROTENUTO, F., ERONEN, J. T. and FORTELIUS, M. 2011. Longer in the tooth, shorter in the record? The evolutionary correlates of hypsodonty in Neogene ruminants. *Proceedings of the Royal Society B*, **278**, 3474–3481.

RENAUD, S., LEDEVIN, R., PISANU, B., CHAPUIS, J.-L., QUILLFELDT, P. and HARDOUIN, E. A. 2018. Divergent in shape and convergent in function: adaptive evolution of the mandible in Sub-Antarctic mice. *Evolution*, **72**, 878–892.

ROHLF, F. J. 1993. Relative warp analysis and an example of its application to mosquito. *Contributions to Morphometrics*, **8**, 131.

—— and BOOKSTEIN, F. L. 2003. Computing the uniform component of shape variation. *Systematic Biology*, **52**, 66–69.

SANDER, P. M., CHRISTIAN, A., CLAUSS, M., FECHNER, R., GEE, C. T., GRIEBELER, E. M., GUNGA, H.-C., HUMMEL, J., MALLISON, H., PERRY, S. F., PREUSCHOFT, H., RAUHUT, O. W. M., REMES, K., TÜTKEN, T., WINGS, O. and WITZEL, U. 2010. Biology of the sauropod dinosaurs: the evolution of gigantism. *Biological Reviews*, **86**, 117–155.

SANSALONE, G., CASTIGLIONE, S., RAIA, P., ARCHER, M., DICKSON, B., HAND, S., PIRAS, P., PROFICO, P. and WROE, S. 2020. Decoupling functional and morphological convergence, the study case of fossorial mammalia. *Frontiers in Earth Science*, **8**, 112.

SCHALLER, G. B. 1972. *The Serengeti lion: A study of predator-prey relations*. University of Chicago Press, 480 pp.

SCHLAGER, S. and GIRINON, F. 2017. Rvcg: Manipulations of triangular meshes based on the 'VCGLIB' API. v.0.1x. https://cran.r-project.org/web/packages/Rvcg/index.html

—— PROFICO, A., DI VINCENZO, F. and MANZI, G. 2018. Retrodeformation of fossil specimens based on 3D bilateral semi-landmarks: implementation in the R package "Morpho". *PLoS One*, **13**, e0194073.

—— JEFFERIS, G., IAN, D. and SCHLAGER, M. S. 2020. Morpho: Calculations and visualisations related to geometric morphometrics. R package v.2.8. https://cran.r-project.org/web/packages/Morpho/index.html

SERB, J. M., SHERRATT, E., ALEJANDRINO, A. and ADAMS, D. C. 2017. Phylogenetic convergence and multiple shell shape optima for gliding scallops (Bivalvia: Pectinidae). *Journal of Evolutionary Biology*, **63**, 685–1747.

SLATER, G. J. and VAN VALKENBURGH, B. 2008. Long in the tooth: evolution of sabertooth cat cranial shape. *Paleobiology*, **34**, 403–419.

SPEED, M. P. and ARBUCKLE, K. 2016. Quantification provides a conceptual basis for convergent evolution. *Biological Reviews*, **92**, 815–829.

STAYTON, C. T. 2006. Testing hypotheses of convergence with multivariate data: morphological and functional convergence among herbivorous lizards. *Evolution*, **60**, 824–841.

—— 2015. The definition, recognition, and interpretation of convergent evolution, and two new measures for quantifying and assessing the significance of convergence. *Evolution*, **69**, 2140–2153.

VAN VALKENBURGH, B. 2007. Deja vu: the evolution of feeding morphologies in the Carnivora. *Integrative & Comparative Biology*, **47**, 147–163.

WAINWRIGHT, P. C. 2007. Functional versus morphological diversity in macroevolution. *Annual Review of Ecology, Evolution, & Systematics*, **38**, 381–401.

WAKE, D. B., WAKE, M. H. and SPECHT, C. D. 2011. Homoplasy: from detecting pattern to determining process and mechanism of evolution. *Science*, **331**, 1032–1035.

WROE, S. and MILNE, N. 2007. Convergence and remarkably consistent constraint in the evolution of carnivore skull shape. *Evolution*, **61**, 1251–1260.

—— McHENRY, C. and TOMASON, J. J. 2005. Bite club: comparative biteforce in big biting mammals and the

prediction of predatory behaviour in fossil taxa. *Proceedings of the Royal Society B*, **272**, 619–625.

—— LOWRY, M. B. and ANTÓN, M. 2008. How to build a mammalian super-predator. *Zoology*, **111**, 196–203.

—— CHAMOLI, U., PARR, W. C., CLAUSEN, P., RIDGELY, R. and WITMER, L. 2013. Comparative biomechanical modeling of metatherian and placental saber-tooths: a different kind of bite for an extreme pouched predator. *PLoS One*, **8**, e66888.

ZELDITCH, M. L., SWIDERSKI, D. L. and SHEETS, H. D. 2012. *Geometric morphometrics for biologists: a primer*. Academic Press.